Bull. Mater. Sci. (2023)46:83
https://doi.org/10.1007/s12034-023-02913-7

ZnO–TiO_2/rGO heterostructure for enhanced photodegradation of IC dye under natural solar light and role of rGO in surface hydroxylation

KHAOULA KACEM[1,2], JUAN CASANOVA-CHAFER[3], ABDESSALEM HAMROUNI[4], SAMI AMEUR[2,5], FRANK GÜELL[6], MOHAMED FAOUZI NSIB[1,2,*] and EDUARD LLOBET[3]

[1]Higher School of Sciences and Technology of Hammam, University of Sousse, 4011 Sousse, Tunisia
[2]NANOMISENE Laboratory, LR16CRMN01, Centre for Research on Microelectronics and Nanotechnology (CRMN), Technopole of Sousse, B.P 334, 4054 Sousse, Tunisia
[3]Universitat Rovira i Virgili, MINOS, Avda. Països Catalans, 26, 43007 Tarragona, Spain
[4]Research Unit Catalysis and Materials for the Environment and Processes URCMEP, National School of Engineers of Gabes, University of Gabes, University Campus, 6072 Gabes, Tunisia
[5]High Agronomic Institute of Chott Meriem, University of Sousse, 4042 Sousse, Tunisia
[6]ENFOCAT-IN2UB, Universitat de Barcelona, 08028 Barcelona, Spain
*Author for correspondence (mohamed.faouzi.ncib@gmail.com)

MS received 17 October 2022; accepted 16 January 2023

Abstract. To overcome the limitations of ZnO as a photocatalyst, the present work reports a ternary nanocomposite (ZnO–TiO_2/rGO) with a high photocatalytic activity under direct natural solar light irradiation. Reduced graphene oxide (rGO) was obtained after bio-reduction of GO using pomegranate peels. Techniques of FE-SEM, TEM, XRD, FTIR, UV–Vis DRS, Raman and PL were used for characterization purpose. The ternary nanocomposite exhibited a high photocatalytic activity towards the degradation of indigo carmine dye, resulting in an efficiency of 92% within 150 min under sunlight illumination. Accordingly, the hybridization of ZnO with TiO_2 and rGO improves light absorption, promotes high separation of photogenerated charges, and solves the photocorrosion drawback of ZnO, leading to a better stability and reusability of the nanocomposite. Particularly, the prepared rGO allowed certain hydrophilicity and a better surface hydroxylation. In view of that, a comprehensive photocatalytic mechanism was proposed and discussed, referred to experiments showing the effect of holes and $^{\bullet}OH$ scavengers. The findings revealed that the developed rGO hybridized with ZnO–TiO_2 heterojunction can be a promising candidate for removing environmental contaminations using natural solar light.

Keywords. ZnO–TiO_2/rGO; photocatalysis; hydroxylation; indigo carmine; solar light.

1. Introduction

Water contamination is a major societal concern worldwide. Freshwater availability has been progressively reduced due to the unregulated and unrestrained human population and industrialization growth, which have interrupted the natural purifying process [1,2]. According to the World Health Organization (WHO) reports, about 8,29,000 people die every year because of diseases from drinking contaminated water, sanitation and hand hygiene. In this context, the use of organic dyes in the textile industry is one of the main activities that pollute water [3,4]. Several dyes such as indigo carmine (IC), methylene blue (MB), methyl orange (MO) and rhodamine B (RhB) have high solubility and stability in water, therefore their ejection in water bodies can lead to hazardous effects for human health and environment [5,6].

Hence, progress in water purification is critical due to the importance of individual health and environmental concerns. Despite that industries use a variety of methods to purify water, most of these techniques present drawbacks such as high energy, operational and maintenance cost, large areas and poor effectiveness [7,8]. In the last decades, photocatalysis has gained a lot of consideration owing to its simplicity, high efficiency and ability to use solar energy as a green and safe energy source for the degradation process and chemical detoxification [9].

ZnO is among the most popular metal oxides that have been studied as photocatalysts. It shows promising features and presents cost-effectiveness, high surface reactivity, photosensitivity and non-toxicity [10–12]. In wastewater medium, the photodegradation process of the organic pollutants in the presence of ZnO nanoparticles (NPs) irradiated with UV light (<400 nm) is mainly

Published online: 20 April 2023

based on the production of hydroxyl radicals (•OH) acting as oxidizing agents. Accordingly, the hydroxyl group (OH) concentration on the photocatalyst surface has a key role in the photodegradation process. Nevertheless, ZnO presents some limitations such as low stability during the photocatalytic process due to the photo-corrosion effect; low visible-light absorption due to its wide bandgap, allowing the absorption of only 5% of the solar light; and quick recombination of electron–hole pairs, leading to poor photocatalytic efficiency under solar light [13,14]. That is why, researchers have suggested many strategies to enhance the photocatalytic performance of ZnO under the visible-light, such as doping with metal ions [15], decorating with noble metals (Ag, Au, Pd) [16,17], and coupling ZnO with other semiconductors such as TiO_2 [18–20]. This last approach consists of the heterojunction engineering that could enhance the separation of the photoinduced charge carriers and consequently boost the production of radicals. Indeed, ZnO and TiO_2 are two n-type semiconductors that are well suited to form heterojunction since the energies of both the conduction (CB) and the valence band (VB) edges of ZnO are slightly higher than the corresponding ones of TiO_2. As a result, for ZnO–TiO_2 heterostructure, electrons are confined in TiO_2, while holes are accumulated in ZnO [18–20].

Recently, the use of graphene derivatives-based nanomaterials in photocatalysis has attracted enormous attention since graphene-based nanomaterials have unique properties, such as high electrical conductivity, a strong capability in accepting electrons and a high surface area [21,22]. Therefore, the combination of ZnO with graphene derivatives is expected to increase the absorption in the visible-light range, facilitate the exposure of large catalytic active sites, and enhance the electron transfer from the CB of ZnO allowing the electron–hole separation [23–25]. Several studies have been reported on the use of ZnO/graphene derivatives for the photocatalytic removal of organic pollutants. Xu *et al* [26] reported that the hybridization of 2 wt% of graphene with ZnO improves the photocatalytic efficiency of pure ZnO by almost five times. Atchudan *et al* [27] demonstrated that ZnO/GO exhibited much higher photocatalytic activity in the degradation of methylene blue (MB) under UV-light irradiation (98.5% after 15 min of irradiation) compared to pure ZnO (49% after 60 min of irradiation). Prabhu *et al* [28] developed ZnO/rGO nanocomposites for the photocatalytic degradation of dyes under UV–vis light irradiation. It was found that 3 wt% reduced graphene oxide (rGO)-loaded ZnO (ZnO-3%rGO) showed higher photocatalytic performance than pure ZnO [28]. Ramos *et al* [29] investigated the photocatalytic activity of ZnO/rGO nanorods (NRs) through the degradation of methyl orange (MO) and showed that coupling ZnO with rGO improved the photodegradation efficiency compared to pure ZnO. Most of the mentioned studies regarding the use of ZnO as a photocatalyst were carried out under artificial UV irradiation, however, its application under natural solar light irradiation still limited. More importantly, most of these studies did not show or precise the genuine role of rGO in improving the photocatalytic efficiency of the prepared materials. Although GO is usually partially reduced, and certain oxygen functionalities are maintained in its surface, the hydrophobic–hydrophilic properties of the obtained rGO were not discussed.

In view of this, we present here the first use of a ternary nanocomposite ZnO–TiO_2/rGO for the degradation of IC under direct natural solar light. It is anticipated that the combination of the ZnO–TiO_2 heterojunction with rGO can enhance the photocatalytic performance of ZnO and make it an efficient photocatalyst under direct solar light. ZnO–TiO_2 heterojunction was synthesized through the sol–gel method. GO was fabricated by the commonly used modified Hummer's method and bio-reduced, for the first time, using pomegranate peels bio-extract to obtain rGO. It is shown that the partial reduction of GO allows certain hydrophilicity of the ZnO–TiO_2/rGO surface, leading to higher •OH production and then better photocatalytic activity.

2. Experimental

2.1 *Synthesis of GO and rGO*

The oxide (GO) and reduced form (rGO) of graphene were synthesized following our previous work [30]. Briefly, a modified Hummers' method was used to synthesize GO from natural graphite powder and pomegranate peels bio-extract was used as a reducing agent for the preparation of rGO (figure 1).

2.2 *Synthesis of ZnO–TiO_2*

The sol–gel technique was selected for the synthesis of the ZnO–TiO_2 heterostructure. Accordingly, we dissolved separately 4.65 g of titanium isopropoxide ($Ti[OCH(CH_3)_2]_4$, Sigma Aldrich) and 3 g of zinc acetate dihydrate ($Zn(CH_3COO)_2.2H_2O$, Sigma Aldrich) in 10 ml of isopropanol (C_3H_7OH, 99.8%, Sigma Aldrich). After that, both solutions were mixed by adding dropwise the zinc acetate solution to that of titanium isopropoxide, and the obtained mixture was stirred for 10 min. Subsequently, 3 ml of acetic acid (CH_3COOH, Sigma Aldrich) and 7 ml of distilled water were added to the mixture, which was further stirred constantly at 70°C for 15 min. Finally, the precipitate obtained after filtration and rinsing operations was then dried at 90°C overnight and annealed at 400°C for 3 h in static air to get ZnO–TiO_2 powder.

Pure ZnO and TiO_2 were synthesized separately by following the same procedure and conditions but without mixing the solutions.

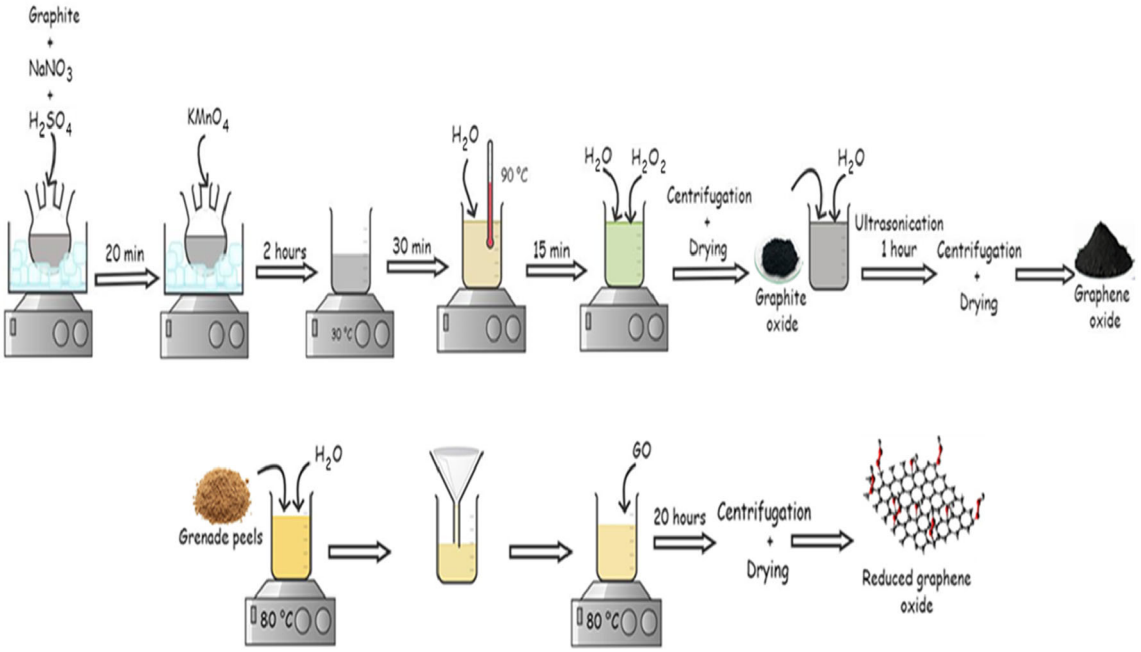

Figure 1. Schematic illustration of GO and rGO syntheses.

2.3 *Synthesis of the ternary ZnO–TiO_2/rGO nanocomposite*

To synthesize this composite, an amount of 30 mg of rGO (1% wt to ZnO–TiO_2) was firstly dispersed in 50 ml of distilled water using an ultrasound path during 1 h. Then, 3 g of ZnO–TiO_2 powder was added and the resulting mixture was inverted and stirred alternately (10 min each) over 1 h. Next, the system was separated using centrifugation and the precipitate was rinsed with distilled water, and dried at 90°C for one night which finally resulted in the ZnO–TiO_2/rGO nanocomposite.

The ZnO/rGO composite was prepared by following the same protocol.

2.4 *Photocatalytic experiments*

The photocatalytic activities of the prepared nanomaterials and the experiments' reaction conditions were carried out according to our previous work, illustrating the photodegradation of IC dye under direct sunlight, in the presence of ZnO/rGO [30]. Experiments were carried out in Sousse city (East of Tunisia) in June when the sky is clear, and the climate is relatively hot (30–32°C). Briefly, 25 mg of powdered nanocomposites were dispersed in 50 ml of IC mixture and placed in the dark with stirring during 45 min to achieve adsorption and desorption equilibrium. Subsequently, the reactor was exposed to direct sunlight for 150 min while stirring continuously. Samples were collected from the mixture at regular intervals, centrifuged and examined by UV–visible spectroscopy.

The total percentage of IC photodegradation was determined using the following equation:

$$\text{Degradation}\,(\%) = [(C_0 - C)/C_0] * 100,$$

where C_0 corresponds to the IC concentration after 45 min in the dark, and C the concentration of IC at a given time within the photocatalytic process.

Similar tests were performed out in the presence of 2 mmol of tert-butanol (TB) and ethylenediaminetetraacetic acid (EDTA), which are designated as $^{\bullet}OH$ radicals and holes scavengers, respectively.

2.5 *Materials characterization*

Different experimental techniques were used to investigate the physical, optical and chemical characteristics of the as-prepared materials. The morphological structure of the samples was examined employing transmission electron microscopy (TEM, JEOL JEM 2100F) and field emission scanning electron microscopy (FESEM, Carl Zeiss AG - ULTRA 55). The elemental composition of the prepared nanomaterials was examined by energy dispersive X-ray (EDX) spectroscopy. Fourier transform infrared was used to study the composition of the different samples within the wavelength range of 4000–400 cm^{-1} using a FTIR spectroscopy (FTIR, Perkin Elmer UATR two). Besides, Raman spectroscopy was recorded to investigate the structure and quality of the nanocomposites employing a Raman spectrometer (Renishaw plc) connected with a coupled confocal Leica DM2500 microscope applying a green laser at the wavelength of 514 nm. The optical properties and bandgap

values of the samples were investigated using UV–vis diffuse reflectance spectroscopy (Shimadzu UV 2600/2700 spectrophotometer) coupled with an integrating sphere. A $BaSO_4$ standard was used to calibrate the instrument. The photoluminescence (PL) measurements at ambient temperature were performed employing a chopped Kimmon IK Series He-Cd laser (325 nm and 40 mW). The dispersion of fluorescence was made with a monochromator (Oriel Corner Stone 1/8 74000), identified through a Hamamatsu H8259-02 equipped with a photomultiplier (socket assembly E717-500), and amplified with a Stanford Research Systems (SR830 DSP). Light was scattered using a 360 nm filter. All spectra were adjusted for the response function of the devices. Finally, X-ray diffraction (XRD, Philips X'Pert) using a copper source (Cu-Ka radiation, = 0.154187 nm) in the 2θ range of 5–80° was used to identify the crystallinity and structure of the samples.

3. Results and discussion

3.1 *FESEM analysis*

The surface morphology of the prepared pure ZnO and ZnO–TiO_2 heterostructure was examined by FESEM. Figure 2a shows a non-homogenous surface of ZnO with the presence of irregularly shaped clusters of NRs and NPs. Figure 2b shows both ZnO and TiO_2 nanomaterials, which are almost uniformly distributed throughout the surface, possibly due to homogeneous distribution during the synthesis of ZnO–TiO_2 nanocomposite.

The elemental composition of the ZnO–TiO_2 heterostructure was examined using the EDS technique (figure 2c). Zn, Ti and O elements are clearly shown, indicating the successful formation of a high-quality ZnO–TiO_2 heterostructure. The Zn signal should come primarily from ZnO, whereas the signal for Ti originates from TiO_2 nanoparticles. The weak signal of C should originate from the diamond support used to deposit the films. Elements weight percent show mainly 6.08% C, 53.72% O, 16.76% Ti and 23.45% Zn. These findings show that a composite of two-phase formation from ZnO and TiO_2 nanomaterials led to the formation of S–S heterojunction on the surface of the two materials. Conversely, the low content of rGO in ZnO/rGO and ZnO–TiO_2/rGO nanocomposites preclude its observation in both samples.

3.2 *TEM analysis*

The TEM images of rGO, ZnO, ZnO/rGO, ZnO–TiO_2 and ZnO–TiO_2/rGO are shown in figure 3. Figure 3a shows the rGO layers folded together, whereas figure 3b shows the ZnO NRs in parallel with the existence of ZnO NPs of hexagonal morphology. The ZnO/rGO nanocomposite is depicted in figure 3c. This indicates the presence of rGO layers decorated with ZnO NRs and NPs clusters. Figure 3d shows TEM images of the calcined ZnO–TiO_2 sample, which is composed of TiO_2 NPs and ZnO NRs and NPs at a lower resolution. In figure 3e, we can easily differentiate the existence of all components in the ternary ZnO–TiO_2/rGO nanocomposite: small spherical nanoparticles of TiO_2 (diameter under 10 nm), clusters of ZnO NPs and NRs (dimensions under 100 nm) and rGO sheets. These results give clear evidence for the anchoring of both ZnO and the binary ZnO–TiO_2, respectively, on the rGO.

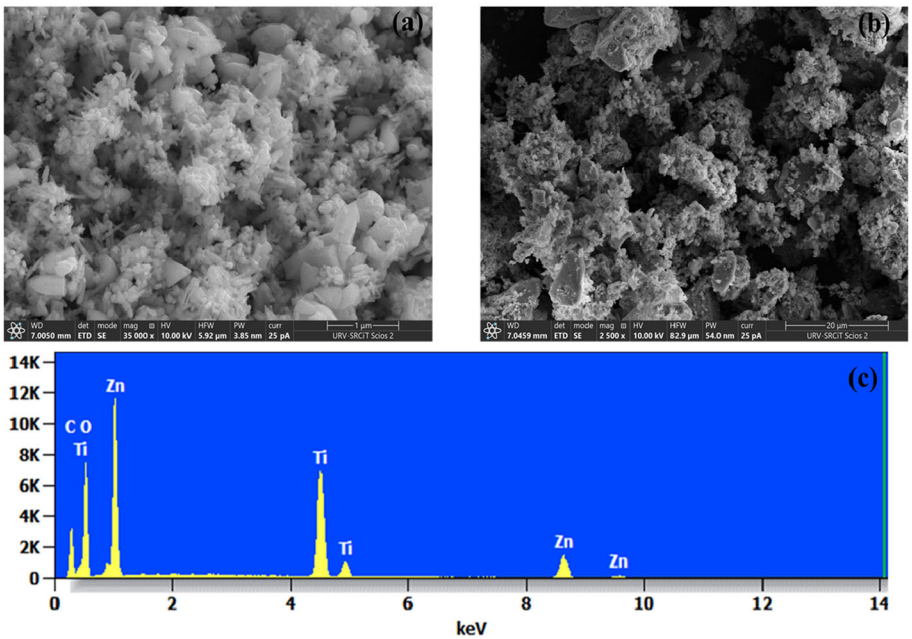

Figure 2. FESEM images of (**a**) ZnO and (**b**) ZnO–TiO_2. (**c**) EDX analysis of ZnO–TiO_2.

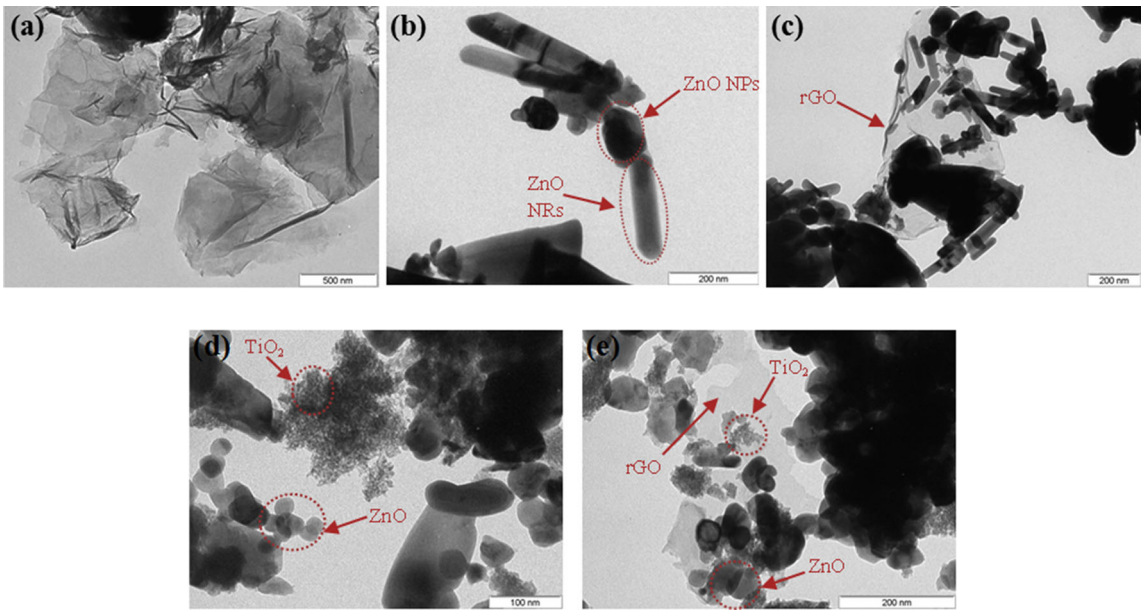

Figure 3. TEM images of (**a**) rGO, (**b**) ZnO, (**c**) ZnO/rGO, (**d**) ZnO–TiO_2 and (**e**) ZnO–TiO_2/rGO.

3.3 *X-ray diffraction analysis*

Figure 4 presents the XRD patterns of the prepared samples. Thus, in the XRD pattern of rGO a broad peak (001) was observed at 2θ = 25.3°. Pure ZnO presents characteristic peaks at around 2θ = 31.8, 34.44, 36.28, 47.55, 56.62, 62.88, 66.4, 67.95 and 69.1°, which are referenced to the crystal lattices of (100), (002), (101), (102), (110), (103), (200), (112) and (201), respectively [5]. The position of these diffraction peaks indicates that the obtained ZnO has a hexagonal wurtzite structure (Joint Committee on Powder Diffraction Standards (JCPDS) No. 36-1451). Additionally, the diffraction peaks of pure TiO_2 at approximately 2θ = 25.42, 38.22, 48.02, 54.94, 62.58, 69.98 and 75.88, indexed to (101), (004), (020), (105), (213), (116) and (215) crystal planes, respectively [31], reveal that the prepared TiO_2 corresponds to the anatase crystalline phase (JCPDS No. 21-1272).

The XRD pattern of the binary ZnO–TiO_2 nanocomposite exhibits diffraction peaks with low intensity at 2θ values of 31.8, 34.4, 36.28, 47.61, 56.64, 62.9 and 67.95°, which correspond to the ZnO wurtzite structure [32]. However, the characteristic peaks of the anatase TiO_2 disappeared in the XRD pattern of ZnO–TiO_2 sample. The reflections observed at 2θ = 35.3, 56.8 and 62.3° can be matched with those of an impurity phase of zinc titanate ($ZnTiO_3$) (JCPDS No. 26-1500), resulting from the reaction between titania and zinc oxide [33]. Many reasons can be mentioned to explain the absence of TiO_2 peaks in the ZnO–TiO_2 XRD pattern. Firstly, it can be suggested that some Ti^{4+} cations can incorporate into the ZnO network, which is confirmed by the fact that the ionic radii of Ti^{4+} (60.5 pm) and Zn^{2+} (60 pm) are comparable, inhibiting the production of the TiO_2 crystalline structure [34].

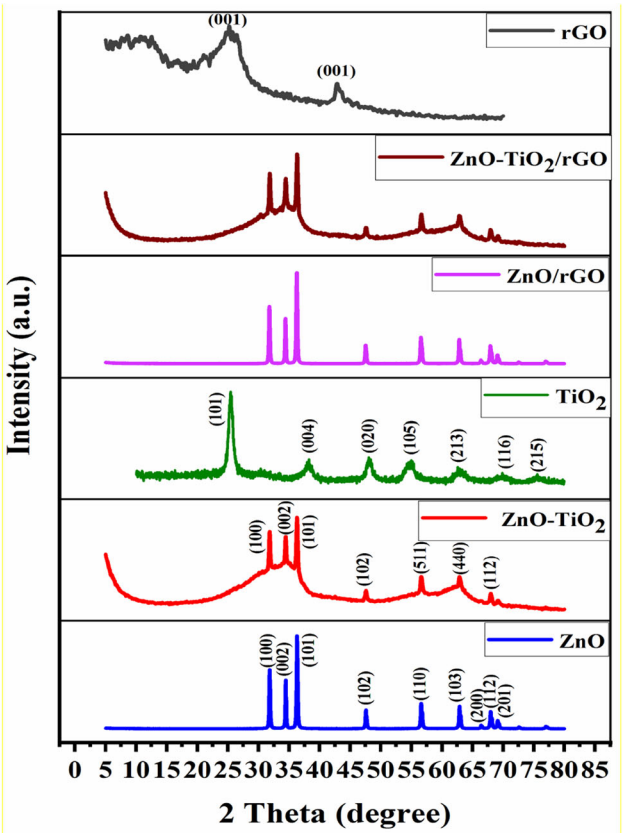

Figure 4. XRD patterns of rGO, ZnO, TiO_2, ZnO–TiO_2, ZnO/rGO and ZnO–TiO_2/rGO.

The second reason can be related to the amount of ZnO nanoparticles added during the sol–gel process, since a small excess of these nanoparticles can prevent the crystallization process during the heating procedure, leading to

the vanishment of the crystal structure of TiO_2 [18,34,35]. In fact, coupling two semiconductors may decelerate the growth of each semiconductor particles but not blocking (preventing). Maybe kinetically, the TiO_2 particles were so slow to be formed corresponding to the ZnO particles formation (which start from 160°C).

On the other hand, the rGO diffraction peaks did not appear in the ZnO/rGO and the ZnO–TiO_2/rGO XRD patterns, owing to the low amount of rGO in both prepared nanocomposites [35]. Nonetheless, the successful incorporation of rGO in these nanocomposites was proved through TEM and Raman studies.

3.4 *FTIR spectroscopy*

Infrared spectra of the prepared pure oxides (ZnO and TiO_2) and the TiO_2–ZnO/rGO nanocomposite are reported in figure 5. Each of the ZnO and TiO_2 spectra showed a broad and intense band at around 450 cm^{-1}, attributed to the Zn–O and Ti–O bonds, respectively. This band is obviously present in the spectrum of the TiO_2–ZnO/rGO nanocomposite. Besides, the band at 1365 cm^{-1} correspond to C=C bond, evidencing the existence of graphene layers [36]. Moreover, the band observed at 1014 cm^{-1} is attributed to the establishment of M–O–C bond linking the rGO sheets to the metal oxides. On the whole, the presence of bands attributed to the ZnO–TiO_2 and rGO in the synthesized TiO_2–ZnO/rGO proves the effective establishment of the nanocomposite.

Interestingly, a particular presence should be noticed in the spectrum of the TiO_2–ZnO/rGO nanocomposite of the bands at 3448 and 1635 cm^{-1}, arising from the O–H vibration and H–O–H bending vibration, respectively, of adsorbed H_2O molecules, which are absent or very weak in the spectra of the pure oxides. Particularly, the broadening of the O–H band at around 3448 cm^{-1} is attributed to the presence of residual water molecules intercalated between the rGO sheets [37]. This result shows that the prepared rGO improves the affinity of water molecules to the TiO_2–ZnO surface. This suggestion is quite strange since rGO is known as a hydrophobic material [38]. However, as the reduction of GO using phytoextracts of pomegranate peels removed partially the oxygen-containing functional groups, then, low amounts of functional groups still remained at the edge and basal plane of rGO [38]. These residual functional groups are expected to improve the hydrophilicity of the surface, known as a key parameter for the photocatalytic reactions.

3.5 *Optical analysis*

3.5a *Raman spectroscopy:* Raman spectroscopy is a powerful and a non-destructive technique, especially for characterizing graphene-based nanocomposites. In particular, it can be used to perfectly evaluate the degree of disorder in the structure of the nanocomposites by comparing the intensity ratio (I_D/I_G). Therefore, to determine this ratio, we focus on the change of the rGO spectra in the prepared nanocomposites [39]. For that reason, Raman spectra of rGO, ZnO/rGO and ZnO–TiO_2/rGO are displayed in figure 6. Two main bands, D and G, were observed in all spectra of the analysed samples. The D-band corresponds to the first-order scattering of E_{2g} phonons carried out by carbon atoms hybridized sp^2 and then, gives information about the sp^3 defects and disorders in the materials; while the G-band is attributed to the breathing mode of κ-point photons of A_{1g} symmetry and gives information on the presence of sp^2 hybridized C=C bond [8]. For rGO, the D and G bands were detected at 1356 and 1595 cm^{-1}, respectively. The D-band has undergone a shift to 1309 and 1320 cm^{-1}, while the G-band moved to 1596 and 1606 cm^{-1} in the spectra of ZnO/rGO and ZnO–TiO_2/rGO, respectively.

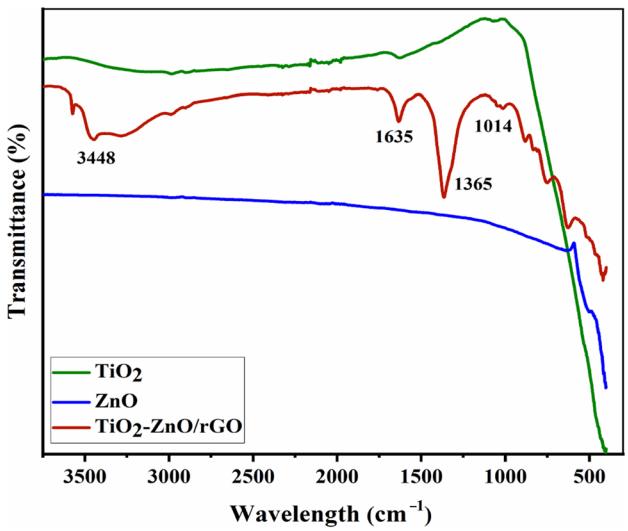

Figure 5. FTIR spectra of ZnO, TiO_2 and TiO_2–ZnO/rGO.

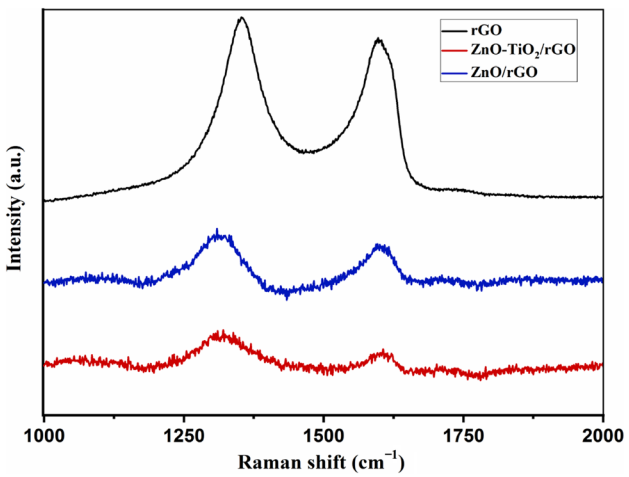

Figure 6. Raman spectra of rGO, ZnO/rGO and ZnO–TiO_2/rGO.

It should be noted that the defect ratio, defined as the ratio of intensities of the D and G bands: I_D/I_G, increased from 1.12 (rGO) to 1.2 (ZnO/rGO) and 1.46 (ZnO–TiO_2/rGO). These results prove the successful attachment of ZnO and the binary ZnO–TiO_2 to rGO leaves, and confirm that the number of defects in the synthesized nanocomposites is higher than that in pristine rGO. The Characteristic defects that could be considered are grain boundaries and vacancies [39–41].

3.5b *UV–vis diffuse reflectance spectroscopy:* The optical properties of the prepared materials were also determined by means of diffuse reflectance spectroscopy (DRS) technique, as shown in figure 7a. It can be noticeably observed that the optical absorption of ZnO–TiO_2/rGO is red-shifted to the visible region (400–800 nm) compared to both ZnO and ZnO–TiO_2. This red-shift is evidently due to the incorporation of rGO, allowing the absorption of light in the visible domain of the spectrum. rGO can also improve the charge carrier separation and decrease their recombination rate. Thus, rGO acts as a photosensitizer allowing the absorption of the visible light and then, the excitation of electrons towards the CB [42].

The direct bandgap energy values of the materials were investigated by extrapolating the linear regime of the Tauc plot determined by considering the samples as indirect semiconductors, as indicated in the following equation:

$$(ahv)^{1/2} = A(hv - E_g), \quad (1)$$

where α, hv, A and E_g are absorption coefficient, absorption energy, proportionality constant and the bandgap energy, respectively.

A bandgap value of 3.14 eV was determined for ZnO–TiO_2 heterostructure, lower than that of pure ZnO (3.2 eV). This modification can be attributed to the creation of new energy states at the ZnO–TiO_2 heterojunction [4]. Furthermore, the E_g value was more decreased to 2.92 eV for the ZnO–TiO_2/rGO nanocomposite (figure 7b). These findings show that the synergetic effect of the semiconductor–semiconductor (S–S) and semiconductor–rGO (S–rGO) heterojunctions clearly decreases the E_g of the ZnO–TiO_2/rGO nanocomposite compared to pristine ZnO and the ZnO–TiO_2 heterostructure. Accordingly, the ternary nanocomposite can serve as an efficient photocatalyst for the degradation of organic pollutants under natural solar light irradiation.

3.5c *PL measurements:* The quantity and type of defects can be evaluated using the photoluminescence (PL) spectra [43]. Figure 8 displays the PL spectra obtained for ZnO, ZnO–TiO_2, ZnO/rGO and ZnO–TiO_2/rGO samples.

By pumping at 325 nm (3.8 eV), a narrow emission band is observed in the UV region at about 390 nm (3.18 eV). This band which corresponds to the near-band edge (NBE) transition is related to the recombination processes of the photogenerated excitons [44]. For the purpose of relative comparison, the intensity of each spectrum was normalized to that of the NBE emission. The NBE band is typically used as an indicator of the crystalline quality of the sample. ZnO shows the maximum emission peak position at around 391 nm (3.17 eV), while for ZnO–TiO_2, ZnO/rGO and ZnO–TiO_2/rGO peaks shifted to 395 nm (3.14 eV), 402 nm (3.08 eV) and 396 nm (3.13 eV), respectively. The full-width at half-maximum of the NBE emission from ZnO, ZnO–TiO_2, ZnO/rGO and ZnO–TiO_2/rGO are around 200,

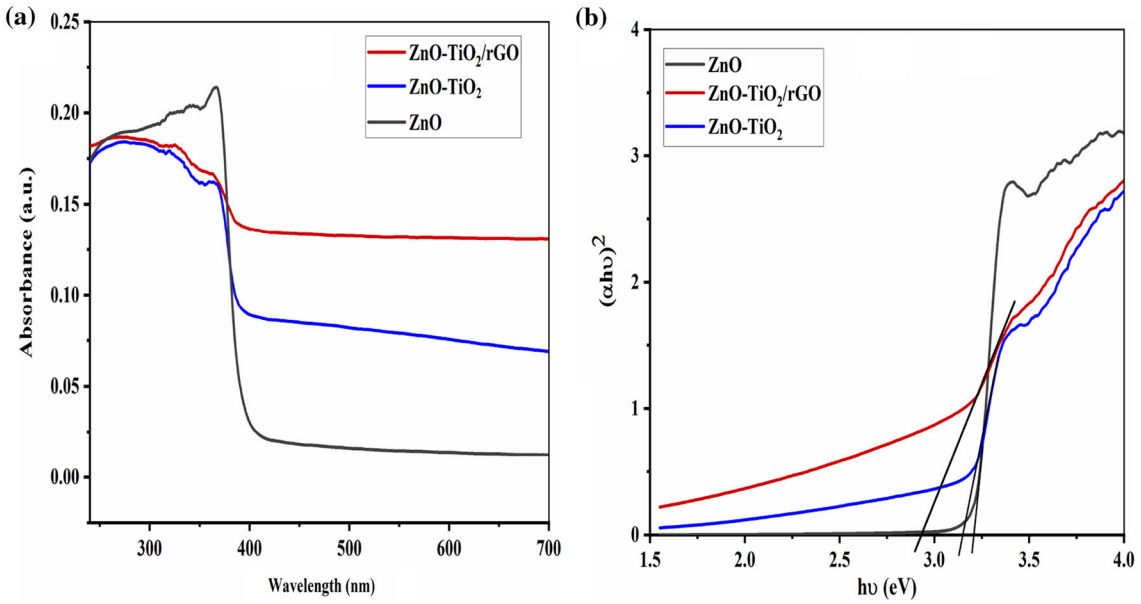

Figure 7. (**a**) Diffuse reflectance spectra in the absorbance mode. (**b**) Tauc plot $(\alpha h\upsilon)^2 = f(h\upsilon)$ for the determination of direct interband transition energies of as-prepared samples.

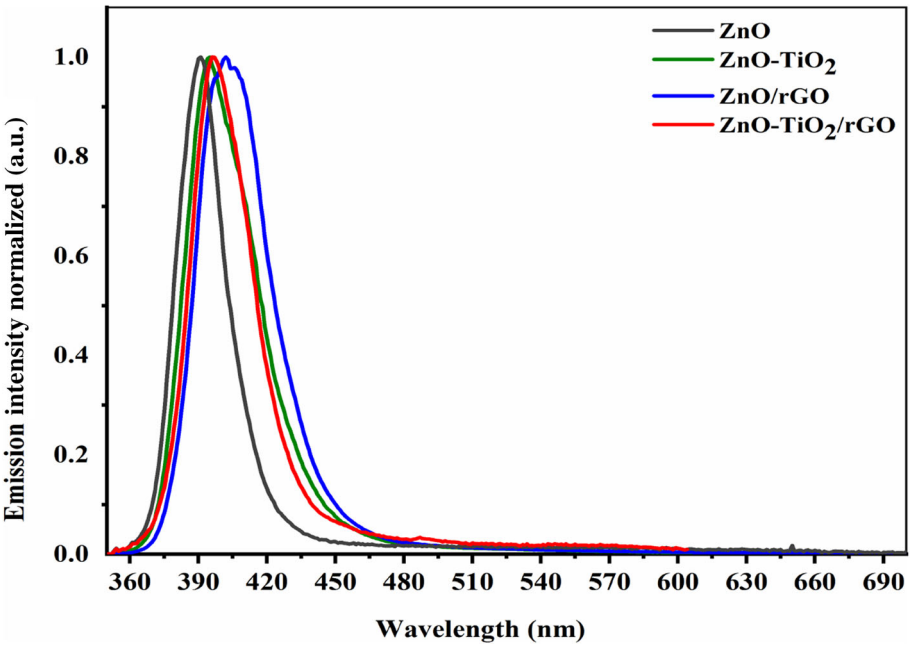

Figure 8. PL spectra of ZnO, ZnO–TiO_2, ZnO/rGO and ZnO–TiO_2/rGO.

280, 270 and 240 meV, respectively. These relatively narrow full-width at half-maximums indicate the good crystalline quality of the samples. These results are consistent with the previous XRD and UV–vis DRS results.

3.6 *Photocatalytic activity*

Figure 9 depicts the photocatalytic degradation of IC dye *vs.* irradiation time. As shown, the self-decomposition (photolysis) of IC can be ignored due to the negligible amount (4.5%) of IC degradation over the 150 min solar light irradiation. After leaving the solution in direct sunlight for 150 min, 42% of initial IC was degraded in the presence of pristine ZnO. This degradation rate was improved to 59% when the ZnO–TiO_2 heterostructure is used. Nevertheless, it can be visibly observed that the degradation rate was significantly improved when rGO was incorporated, leading to 79% for ZnO/rGO and 92% for ZnO–TiO_2/rGO. The amount of rGO in the nanocomposite was selected according to preliminary photocatalytic experimental tests showing that the ZnO–TiO_2/rGO with only 1% exhibits the highest photocatalytic efficiency compared to that of ZnO–TiO_2/0.5%rGO, ZnO–TiO_2/5%rGO. This result confirms that 1% of rGO can be considered as the optimum loading amount in the ZnO–TiO_2 heterostructure.

Figure 10a shows the time variation of the absorption spectrum of IC using ZnO–TiO_2/rGO under sunlight. As it is displayed, the intensity of the absorption peak (at 610 nm) of the IC solution declines progressively and almost disappears after 150 min in the sun, in addition to the blue colour of the solution (figure 10b).

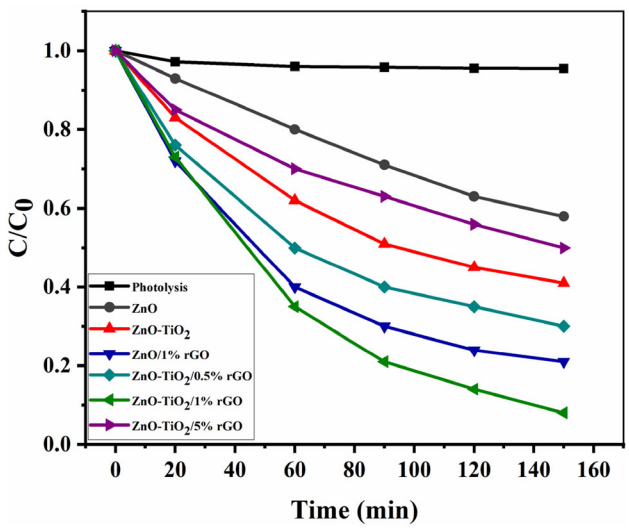

Figure 9. IC photodegradation rate under solar light irradiation as a function of time in the presence of various photocatalysts.

These results show that the synergetic effect of both S–S and S–rGO heterojunctions leads to higher photocatalytic performances. In particular, this progress can be attributed to the incorporation of rGO films permitting better absorption of visible light and higher electronic conductivity than materials without rGO. These latter distinctive properties of rGO allow the increase of the absorption edge of ZnO–TiO_2 into the visible-light region, favour the separation of photogenerated electron–hole pairs and prevent their possible recombination [36,45,46].

Compared to previously reported photocatalysts for IC degradation (table 1), the synthesized ZnO–TiO_2/rGO

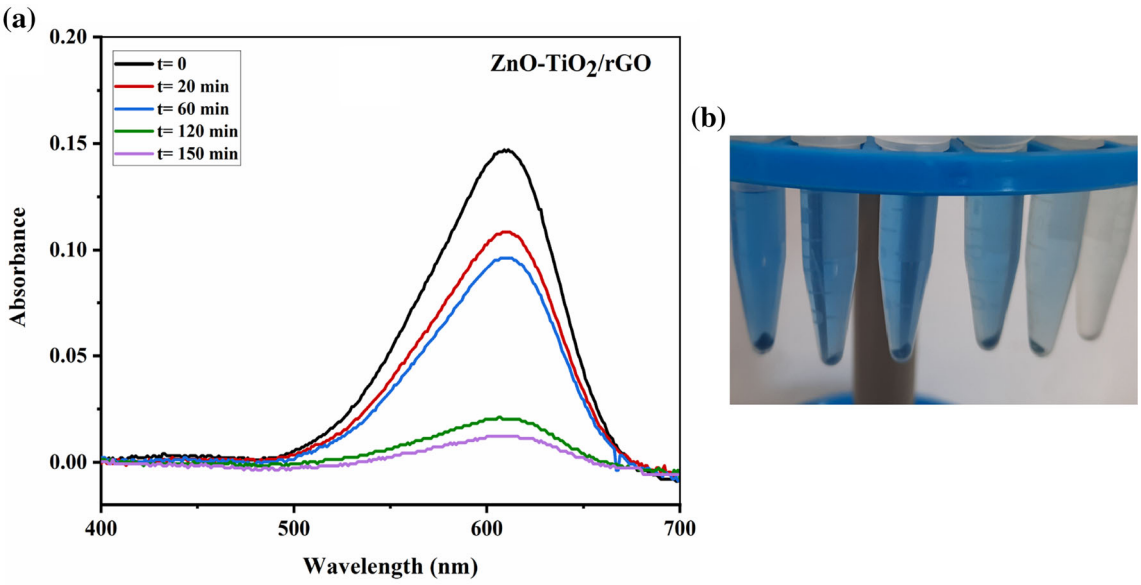

Figure 10. (**a**) Evolution of the UV–vis absorption spectrum of IC solution over the time of degradation by ZnO–TiO_2/rGO under solar light. (**b**) Colour change of IC solution during the photodegradation reaction.

Table 1. Comparison of photocatalytic performance of various photocatalysts for IC degradation (C_{IC} = 20 mg l^{-1}).

Sample	Concentration of photocatalyst (mg ml^{-1})	Irradiation time (min)	Light source	Photocatalyst efficiency (%)	Ref.
ZnO–TiO_2/rGO (1% rGO)	0.5	150	Solar light	92	This work
			Solar simulator	98	
Nd–TiO_2–GO (0.6% Nd)	1	180	Solar simulator	92	[47]
Eu–TiO_2–GO (0.6% Eu)	1	210	Solar light	92.6	[48]
Nd–ZnO–GO (0.3% Nd)	1	210	Solar simulator	95	[49]
0.5% Co–ZrO_2–MWCNTs	1	180	Solar simulator	98	[50]
Pd–ZnS/rGO (1.0% Pd)	1	210	Solar simulator	100	[51]

showed outstanding photocatalytic efficiency under solar light irradiation, since we have used a smaller amount of photocatalyst to degrade IC in a shorter duration.

On the other hand, it is well-known that the photoinstability of ZnO due to the photocorrosion reaction is among the most important limitations to its use in industrial applications as an effective photocatalyst in aqueous solutions [50]. Two main reasons were reported responsible for the ZnO photocorrosion: (i) the interaction between the surface oxygen and holes, and (ii) the surface defects of ZnO which serve as activation sites [50]. However, TiO_2 and rGO are considered as chemically stable.

In view of that, it is expected that the hybridization of ZnO with rGO and TiO_2 could provide protection against its photocorrosion, leading to better photostability. For that reason, the reusability of ZnO–TiO_2/rGO which revealed the highest photocatalytic efficiency among the prepared samples was evaluated through three photodegradation cycles. After each photocatalytic test, the solution was centrifuged, washed with distilled water, and dried to recover the ZnO–TiO_2/rGO powder. Interestingly, figure 11 shows that more than 86% of the photocatalytic performance of the nanocomposite remained after three cycles. This result proves that coupling ZnO with TiO_2 and rGO limits its dissolution reaction during the photocatalytic process under solar light. The slight decrease may be due to the loss content of the photocatalyst during the washing process after each photocatalytic cycle [36,52]. Subsequently, the ternary ZnO–TiO_2/rGO heterostructure can be considered as a stable photocatalyst in aqueous solutions under natural solar light.

3.7 *Photocatalytic mechanism*

On the whole, the performance of the TiO_2–ZnO/rGO photocatalyst is attributed to an extension in the range of light absorption, reduction of electron–hole recombination and to the surface properties. Many considerations are to be taken in account to explain this performance:

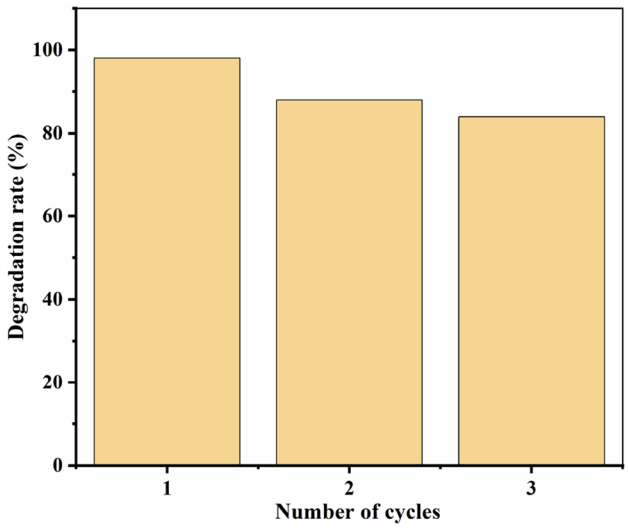

Figure 11. Photodegradation rate of IC by ZnO–TiO_2/rGO after three cycles.

Firstly, the presence of surface defectivity, showed by Raman analysis, induces affinity of the TiO_2–ZnO/rGO sample for water molecules, as also shown in FTIR spectra. In particular, this leads to a higher degree of surface hydroxylation although the rGO is known to be hydrophobic. As mentioned above, the partial reduction of the graphene oxide allows the surface of the TiO_2–ZnO/rGO nanocomposite to have certain hydrophilicity. In this context, the hydroxyl groups have two main roles: (i) they constitute available sites for the substrate favouring the adsorption of IC molecules, and (ii) act as traps for the photoinduced charge carriers resulting in high rate of hydroxyl radical formation during light exposure. These aspects are expected to enhance the photocatalytic activity.

To better understand the basics of this performance in relation to the incorporation of the rGO in the nanocomposite, supplementary photocatalytic experiments were conducted to elucidate the role of the presumed radicals in the photodegradation of IC. For this reason, the photoactivity of the TiO_2–ZnO/rGO sample was experimented in the presence of substances such as tert-butanol to scavenge $^{\bullet}$OH radicals and ethylenediamine tetraacetic acid (EDTA), to scavenge holes [53]. The role of the selected scavengers is to react with a specific radical, producing stable species. The condition is to not interfere with the reaction in order to exclude the effect of this radical in the degradation. Holes are usually scavenged by electron donor species, whereas $^{\bullet}$OH radicals are scavenged by electron acceptors. Figure 12 shows the effect of the selected scavengers on the photocatalytic performance of both TiO_2–ZnO and TiO_2–ZnO/rGO samples.

It can be observed that the addition of the alcohol (tert-butanol), as $^{\bullet}$OH scavenger, to the IC solution, has decreased the photocatalytic performance of the TiO_2–ZnO/rGO from 92 to 61% after 150 min of solar irradiation. This decrease was found to be clearly lower in the presence of the TiO_2–ZnO heterostructure, showing variations from 59 to 48%. These results suggest both things: (i) the hydroxyl radicals have an important contribution in the redox reactions during the photocatalytic removal of IC dye, and (ii) the surface hydroxylation of the TiO_2–ZnO/rGO is higher than that of the TiO_2–ZnO heterostructure, as already shown by FTIR analysis.

On the other hand, the presence of EDTA, as a holes snare, was shown to decrease the photocatalytic efficiency of TiO_2–ZnO/rGO from 92 to 81%, lower than that resulted after addition of the $^{\bullet}$OH scavenger (tert-butanol). This finding suggest that the $^{\bullet}$OH radicals are generated not only in the VB by the photogenerated holes, but also in the CB after reaction of the photogenerated electrons with O_2 and H_2O molecules in the solution.

Accordingly, the prepared rGO has a double role in the photocatalytic efficiency of the ZnO–TiO_2/rGO nanocomposite: (i) it allows certain hydrophilicity of the surface leading to better hydroxylation, and (ii) acts as a trap for the photogenerated electrons, which avoids their recombination with the holes.

Following the above results and discussion, a reasonable mechanism of photoactivity of ZnO–TiO_2/rGO under direct sunlight is presented and schematically illustrated in figure 13. Upon exposing to sunlight, the ternary nanocomposite absorbs photons having sufficient energy, causing excitation of electrons (e^-) from VBs of ZnO and TiO_2 to their CBs; at the same time, holes (h^+) are created in their VBs. Owing to the stepwise energy levels of ZnO CB > TiO_2 CB > rGO CB [54], the photoinduced electrons move from the CB of ZnO to the CB of TiO_2 and then to the rGO sheets, as an electron acceptor. This path of electronic transfer inhibits the electron–hole pair recombination and improves the photocatalytic efficiency [55]. After that, the

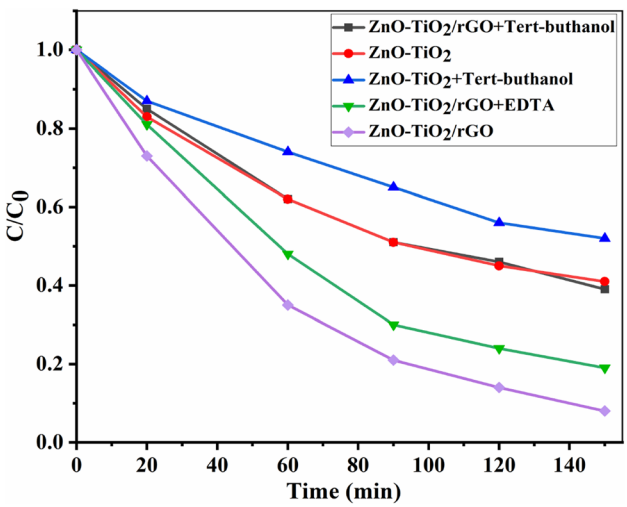

Figure 12. Effect of holes and $^{\bullet}$OH scavengers on the photocatalytic performance of TiO_2–ZnO/rGO and TiO_2–ZnO towards the degradation of IC dye.

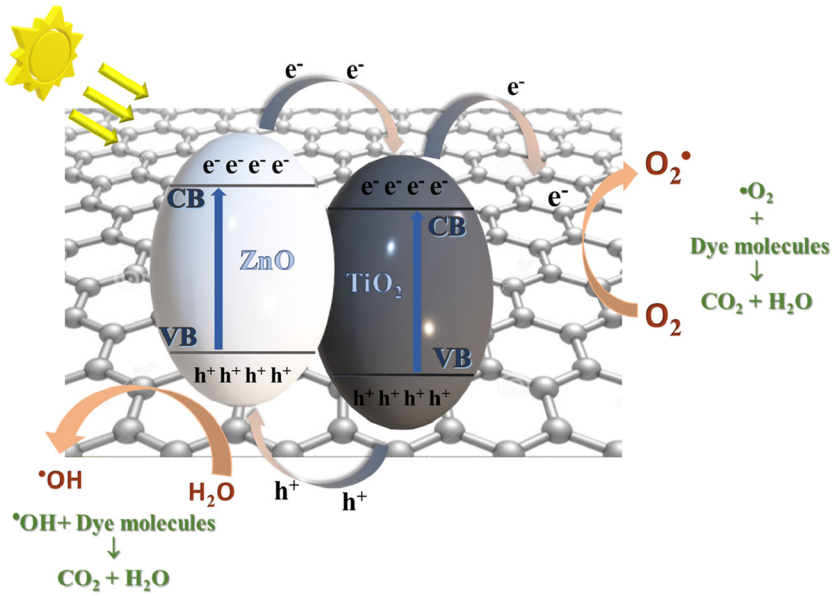

Figure 13. Proposed mechanism of the photocatalytic activity of ZnO–TiO_2/rGO nanocomposite under solar light.

photogenerated electrons react with O_2 and H_2O molecules in the solution to form $O_2^{\bullet}$ radicals, which can be transformed to hydroxyl radicals $^{\bullet}OH$. Meanwhile, the created holes are moved in an inverse way from the VB of TiO_2 to the VB of ZnO before reacting with H_2O, giving arise also to $^{\bullet}OH$ radicals. Finally, the generated radicals are available to oxidize the IC dye to CO_2, H_2O and inorganic anions [54].

4. Conclusion

In summary, a ternary ZnO–TiO_2/rGO nanocomposite was synthesized using a simple chemical approach for the efficient photodegradation of the IC dye under direct solar light. In this nanocomposite, we combine the effect of both S–S and S–rGO heterojunctions to enhance the photocatalytic performance of ZnO. As confirmed by the characterization techniques, the incorporation of rGO with ZnO–TiO_2 improved the visible-light absorption, electron transfer and charge separation. In particular, the prepared rGO allowed certain hydrophilicity, leading to a better surface hydroxylation, and then, to higher production of $^{\bullet}OH$ radicals. These latest are showed to have a key role in the photocatalytic activity of the ZnO–TiO_2/rGO and are generated in both VB and CB. Accordingly, the prepared ternary nanocomposite exhibited a higher photocatalytic performance towards the degradation of IC under solar light irradiation compared to pure ZnO, ZnO–TiO_2 and ZnO/rGO. In view of this, the ZnO–TiO_2/rGO is presented as a potential candidate for photocatalytic de-contamination processes under the inexhaustible solar light.

Acknowledgements

Khaoula Kacem acknowledges the University of Sousse for research funding. We also acknowledge Enas Moustafa and Prof. Lluis Marsal for the reusability test. Juan Casanova-Chafer gratefully thanks ICREA ACADEMIA (project: 2018 ICREA ACADEMIA-01-Ajut). Frank Güell acknowledges the financial support of PID2020-116612RB-C32 and MAT2017-87500-P.

References

[1] Thakre K G, Barai D P and Bhanvase B A 2021 *Water Environ. Res.* **93** 2414
[2] Dutta V, Singh P, Shandilya P, Sharma S, Raizada P, Saini A K *et al* 2019 *J. Environ. Chem. Eng.* **7** 103132
[3] Natarajan S, Bajaj H C and Tayade R J 2018 *J. Environ. Sci.* **65** 201
[4] Mousa H M, Alenezi J F, Mohamed I M A, Yasin A S, Hashem A-FM and Abdal-Hay A 2021 *J. Alloys Compd.* **886** 161169
[5] Chen X, Wu Z, Liu D and Gao Z 2017 *Nanoscale Res. Lett.* **12** 143
[6] Zhang W, Zhang Y, Yang K, Yang Y, Jia J and Guo L 2019 *Nanomaterials (Basel)* **9** 1671
[7] Tian F, Wu Z, Chen Q, Yan Y, Cravotto G and Wu Z 2015 *Appl. Surf. Sci.* **351** 104
[8] Kumar K V A, Lakshminarayana B, Suryakala D and Subrahmanyam Ch 2020 *RSC Adv.* **10** 20494
[9] Viet T Q Q, Khoi V H, Thi Huong Giang N, Thi Van Anh H, Dat N M, Phong M T *et al* 2021 *Colloids Surf. A* **629** 127464
[10] Raizada P, Sudhaik A and Singh P 2019 *Mater. Sci. Energy Technol.* **2** 509

[11] Ani I J, Akpan U G, Olutoye M A and Hameed B H 2018 *J. Cleaner Prod.* **205** 930
[12] Samadi M, Zirak M, Naseri A, Khorashadizade E and Moshfegh A Z 2016 *Thin Solid Films* **605** 2
[13] Nguyen C H, Tran M L, Tran T T V and Juang R-S 2020 *Purif. Technol.* **232** 115962
[14] Prasannalakshmi P and Shanmugam N 2017 *Mater. Sci. Semicond. Process.* **61** 114
[15] Qi K, Xing X, Zada A, Li M, Wang Q, Liu S *et al* 2020 *Ceram. Int.* **46** 1494
[16] Chauhan P S, Rai A, Gupta A and Bhattacharya S 2017 *Mater. Res. Express* **4** 055004
[17] Wei Y, Shahid M Z, Lyu S, Sun W and Lyu S 2021 *RSC Adv.* **11** 22618
[18] Siwińska-Stefańska K, Kubiak A, Piasecki A, Dobrowolska A, Czaczyk K, Motylenko M *et al* 2019 *Appl. Surf. Sci.* **463** 791
[19] Das A, Kumar P M, Bhagavathiachari M and Nair R G 2020 *Appl. Surf. Sci.* **534** 147321
[20] Gupta D, Chauhan R, Kumar N, Singh V, Srivastava V C, Mohanty P *et al* 2020 *J. Environ. Manage.* **258** 110032
[21] Upadhyay R K, Soin N and Roy S S 2014 *RSC Adv.* **4** 3823
[22] Li X, Yu J, Wageh S, Al-Ghamdi A A and Xie J 2016 *Small* **12** 6640
[23] Jana A and Scheer E 2018 *Langmuir* **34** 1497
[24] Lonkar S P, Pillai V and Abdala A 2019 *Appl. Surf. Sci.* **465** 1107
[25] Al-Rawashdeh N A F, Allabadi O and Aljarrah M T 2020 *ACS Omega* **5** 28046
[26] Xu T, Zhang L, Cheng H and Zhu Y 2011 *Appl. Catal. B: Environ.* **101** 382
[27] Atchudan R, Edison T N J I, Perumal S, Karthikeyan D and Lee Y R 2016 *J. Photochem. Photobiol. B* **162** 500
[28] Prabhu S, Megala S, Harish S, Navaneethan M, Maadeswaran P, Sohila S *et al* 2019 *Appl. Surf. Sci.* **487** 1279
[29] Ramos P G, Luyo C, Sánchez L A, Gomez E D and Rodriguez J M 2020 *Catalysts* **10** 660
[30] Kacem K, Ameur S, Casanova-Chafer J, Nsib M F and Llobet E 2022 *J. Mater. Sci.: Mater. Electron.* **33** 16099
[31] Pragathiswaran C, Smitha C, Mahin Abbubakkar B, Govindhan P and Anantha Krishnan N 2021 *Mater. Today Proc.* **45** 3357
[32] Akyüz D 2021 *Opt. Mater.* **116** 111090
[33] Siwińska-Stefańska K, Kubiak A, Piasecki A, Goscianska J, Nowaczyk G, Jurga S *et al* 2018 *Mater.* **11** 841
[34] Chen Y, Zhang C, Huang W, Yang C, Huang T, Situ Y *et al* 2014 *Surf. Coat. Technol.* **258** 531
[35] Johra F T and Jung W-G 2015 *Appl. Catal. A* **491** 52
[36] Vasilaki E, Katsarakis N, Dokianakis S and Vamvakaki M 2021 *Catal.* **11** 332
[37] Ranjan P, Agrawal S, Sinha A, Rao T R, Balakrishnan J and Thakur A D 2018 *Sci. Rep.* **8** 12007
[38] Hidayah N M S, Liu W-W, Lai C-W, Noriman N Z, Khe C-S, Hashim U *et al* 2017 *AIP Conf. Proc.* 150002
[39] Khurshid F, Jeyavelan M, Hudson M S L and Nagarajan S 2019 *R. Soc. Open Sci.* **6** 181764
[40] Abdolhosseinzadeh S, Asgharzadeh H, Sadighikia S and Khataee A 2016 *Res. Chem. Intermed.* **42** 4479
[41] Paul R, Gayen R N, Biswas S, Bhat S V and Bhunia R 2016 *RSC Adv.* **6** 61661
[42] Oppong SO-B, Opoku F and Govender P P 2019 *Appl. Catal. B* **243** 106
[43] Güell F, Cabot A, Claramunt S, Moghaddam A O and Martínez-Alanis P R 2021 *Nanomater.* **11** 870
[44] Reparaz J S, Güell F, Wagner M R, Callsen G, Kirste R, Claramunt S *et al* 2010 *Appl. Phys. Lett.* **97** 133116
[45] Divya K S, Xavier M M, Vandana P V, Reethu V N and Mathew S 2017 *New J. Chem.* **41** 6445
[46] Sengunthar P, Bhavsar K H, Balasubramanian C and Joshi U S 2020 *Appl. Phys. A* **126** 567
[47] Oppong SO-B, Anku W W, Shukla S K, Agorku E S and Govender P P 2016 *J. Sol-Gel. Sci. Technol.* **80** 38
[48] Oppong SO-B, Opoku F and Govender P P 2021 *Catal. Lett.* **151** 1111
[49] Oppong S O B, Anku W W, Shukla S K and Govender P P 2017 *Res. Chem. Intermed.* **43** 481
[50] Anku W W, Oppong SO-B, Shukla S K, Agorku E S and Govender P P 2016 *Prog. Nat. Sci.: Mater. Int.* **26** 354
[51] Agorku E S, Mamo M A, Mamba B B, Pandey A C and Mishra A K 2015 *Mater. Sci. Semicond. Process.* **33** 119
[52] Gang R, Xu L, Xia Y, Zhang L, Wang S and Li R 2021 *ACS Omega* **6** 3831
[53] Schneider J T, Firak D S, Ribeiro R R and Peralta-Zamora P 2020 *Phys. Chem. Chem. Phys.* **22** 15723
[54] Bao H V, Dat N M, Giang N T H, Thinh D B, Tai L T, Trinh D N *et al* 2021 *Surf. Interfaces* **23** 100950
[55] Johra F T and Jung W-G 2015 *Appl. Catal. A* **491** 52